International Journal of Signal Processing, Image Processing and Pattern Recognition
Vol. 7, No. 6 (2014), pp. 29-40
http://dx.doi.org/10.14257/ijsip.2014.7.6.03

System Simulation Modeling for Near-field Millimeter Wave Synthetic Aperture Imaging Radiometer

Jianfei Chen[1], Yuehua Li[1], Jianqiao Wang[1] and Yuanjiang Li[1,2]

[1]*School of Electronic Engineering and Optoelectronic Technology, Nanjing University of Science and Technology, Nanjing, 210094, China*
[2]*Institute of Electronic and Information, Jiangsu University of Science and Technology, Zhenjiang, 212000, China*
Chenfei050607@126.com, nlglyh2013@sina.cn

Abstract

Due to the fact that theoretical analysis and instrument construction for antenna array of synthetic aperture imaging radiometer (SAIR) are both complicated, and designers usually hope to predict the imaging effect and analysis the influence of relevant parameters of SAIR before the system design. The imaging simulation is a very useful method in the system design of SAIR. This paper is devoted to establishing an accurate imaging model for simulating the process of near-field millimeter wave SAIR. In this model, the target radiation signals and received signals of receivers are represented by the accurate signals in the time domain, which improves the efficiency of this simulation model significantly. The visibility function is collected by the cross-correlation between I/Q signals of the antenna pairs just as the imaging process of the practical SAIR. Some characteristics (such as the coherence between targets, the resolution and no-aliasing FOV of SAIR and so on) are verified by the corresponding 1D and 2D simulation experiments, and the effectiveness of this imaging model is also tested by these simulation experiments. The simulation experiment results show that this model is an efficient, accurate imaging simulation model, and can be employed in the system design of near-field millimeter wave SAIR.

Keywords: *Synthetic aperture, millimeter wave, imaging, simulation modeling, radiometer*

1. Introduction

Passive millimeter-wave imaging techniques are currently receiving considerable attention for short-range imaging, such as the high-resolution observations of personal security, due to their ability to detect concealed weapons through obscuring materials such as clothing, cardboard, plastics, and wood with high spatial resolution. Different from familiar X-ray imaging and other active microwave imaging, passive millimeter-wave imaging is commonly regarded as harmless to humans [1-4]. However, due to the tradeoff between the antenna aperture and spatial resolution, conventional real-aperture millimeter-wave imaging system can't achieve the desired high spatial resolution. For solving this contradiction, the interferometric aperture synthesis imaging technology is developed in the 1980s for radio astronomy initially [5, 6]. Then many SAIRs based on this technology have been proposed in microwave and millimeter-wave band, such as ESTAR, 2D-STAR and MIRAS [7-9]. The basic idea of aperture synthesis technology is to use a thin array composed of small aperture antennas to achieve a large aperture antenna by performing correlation operations in pairs. Each complex correlation value is a sample of the visibility function which, in the ideal case,

ISSN: 2005-4254 IJSIP

is the spatial Fourier transform of the brightness temperature distribution [10]. Thus, the choice of the antenna array shape is very important because it determines the sampling strategy in the space frequency domain. For designing the antenna array and selecting relevant system parameters more reasonable, designers usually hope to predict the imaging effect of SAIR and analysis the influence of the related parameters of synthetic aperture imaging before the system design. Thus, the imaging simulation model becomes a very useful method for designers to design the millimeter wave SAIR. As far as we know, there is not a complete imaging model for simulating the imaging process of near-field millimeter SAIR systematically.

Previous simulation models [11-13] simulate the process that antenna collecting target radiation and outputting antenna temperature. In these models, the practical electric field and voltage signals are represented by the equivalent complex baseband signals [13]. Many characteristics (such as the coherence between targets, the resolution and no-aliasing FOV of SAIR etc.) can not be verified by these simulation models. Actually, these models can be seen as the simulation model after the antenna rather than the real simulation model for simulating the imaging process of SAIR. In addition, these imaging models are established based on the far-field approximation conditions with plane wave. But in the near-field SAIR, the imaging distance usually close to the size of the synthetic antenna aperture. Thus those imaging model are unsuitable for simulating the imaging for near-field SAIR, especially for millimeter wave and the terahertz wave with short wavelength [14]. This paper presents an accurate imaging model in the time domain to simulate the imaging process that include target radiating electromagnetic waves, antenna collecting target radiation and transforming them into IF signals, and antenna array collecting the samples of visibility function. The target radiation signals are described in time domain with mean square proportional to the corresponding radiation brightness temperature. The corresponding phase items are set as a random sequence based on the theory of microwave radiation [15]. Then the output IF signals of each individual receiver are obtained by combination of all target radiation signals. Finally, the compensated visibility function will be outputted after the cross-correlation operation with each antenna pairs. In this model, all the signals are described in the time domain, and more close to the realistic signal transformation of SAIR. Results of the simulation experiments show that the signals are in good agreement with the corresponding theoretical result. Moreover, this model can be employed in SAIR system-level simulator design. Thus this proposed imaging model is flexible and suitable for the imaging simulation of near-field SAIR.

This paper is divided into 5 parts. In part-2, the numerical model of target radiating electromagnetic waves, antenna collecting target radiation and transforming them into IF signal, and antenna array collecting visibility function is built. In part-3, the model of part-2 is validated by comparing the statistical characteristics of target radiation and antenna array output signals with corresponding theoretical analysis. Good agreements between them are obtained. In part-4, the corresponding system-level imaging simulation experiments show that this model can be employed in SAIR system-level simulator design. In part-5, a conclusion is presented.

2. The Simulation Modeling for SAIR

Due to the spherical wave effect of near-field millimeter wave SAIR, we establish the accurate simulation model in Cartesian coordinate system for simulating the imaging process of near-field SAIR. This simulation model is built in the time domain for describing the signals accurately and intuitively. In order to analysis the imaging

process conveniently, the antenna array is set as "T" array. The simulation modeling diagram is shown in Figure 1.

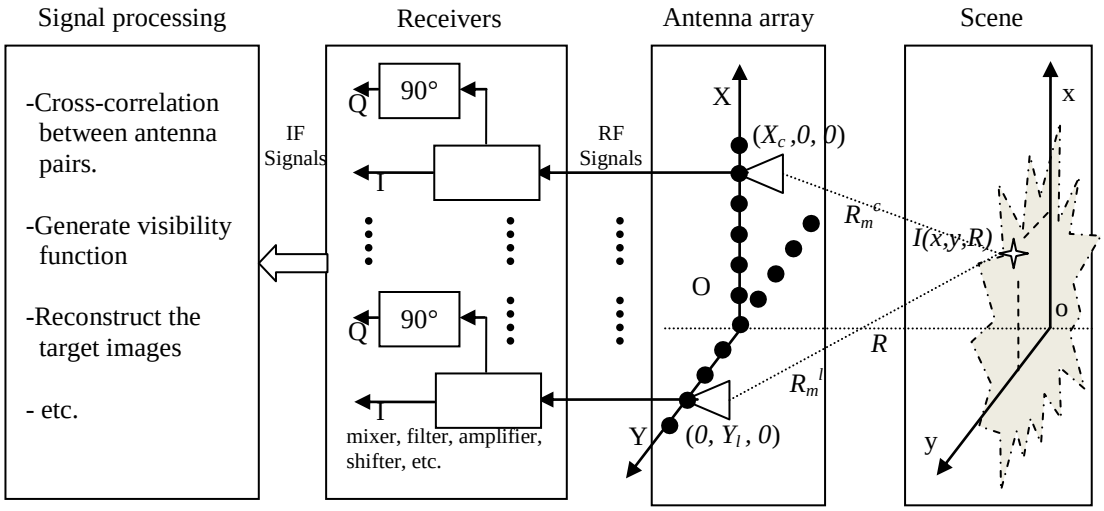

Figure 1. The Simulation Modeling Diagram

As illustrated in Figure 1, the extended target S is located on the scene plane (oxy), with its radiation wave center frequency and wavelength are ω_0 and λ_0 respectively. It is reasonable to assume that the target S is constituted of many discrete point sources. Based on this assumption, the radiation wave generated by the point source S_m located at (x, y) can be expressed as

$$E_m(t) = A_m(t)\cos(\omega_0 t + \varphi_m(t)) \tag{1}$$

Where $A_m(t)$ is the amplitude of S_m and $\varphi_m(t)$ is the corresponding phase information. A_m is proportion to the apparent temperature of source S_m in antennas [13]. The electromagnetic radiation signals are independent of each other in the nature, which means φ_m is an independent distribution function statistically [15]. The antennas are located on $(X_c, 0)$ and $(0, Y_l)$, and the distance between the source S_m and the antennas are $R_m^{\,c}$ and $R_m^{\,l}$. The received signals of the antennas can be expressed as

$$\begin{aligned} E_m^{X_c}(t) &= E_m^{X_c}(t - R_m^c/c)/R_m^c = E_m^{X_c}(t - KR_m^c/\omega_0)/R_m^c \\ &= \frac{A_m}{R_m^c}(t - KR_m^c/\omega_0)\cos(\omega_0 t - KR_m^c + \varphi_m(t - KR_m^c/\omega_0)) \end{aligned} \tag{2}$$

$$E_m^{Y_l}(t) = \frac{A_m}{R_m^l}(t - KR_m^l/\omega_0)\cos(\omega_0 t - KR_m^l + \varphi_m(t - KR_m^l/\omega_0)) \tag{3}$$

Where $K=2\pi/\lambda_0$ is circular wavenumber, c is the speed of electromagnetic wave transmission (the speed of light). Generally the amplitude A_m and phase φ_m are changing slowly with the time for the signals received by the receivers with narrow-band [15]. And the differences of delay time $\Delta\tau=(R_m^{\,c} - R_m^{\,l})/c$ are usually far less than the coherence time [16]. Thus the approximate relation can be obtained as follows

$$A_m(t - KR_m^c/\omega_0) \approx A_m(t - KR_m^l/\omega_0) \approx A_m(t - \tau_0) \tag{4}$$

$$\varphi_m(t - KR_m^c / \omega_0) \approx \varphi_m(t - KR_m^l / \omega_0) \approx \varphi_m(t - \tau_0) \tag{5}$$

Where τ_0 is a time constant, which is set as $[max(R_m^c, R_m^l)+min(R_m^c, R_m^l)]/2$ in this model. Generally, the target is a stationary and stable target, which means that the radiation field of the target scene is a steady radiation field. Based on this condition, we assume that the amplitude function $A_m(t)$ is a constant A_m in the integration time $T\tau$. So Eq.(2) and (3) can be rewritten as

$$E_m^{X_c}(t) = \frac{A_m}{R_m^c}\cos(\omega_0 t - KR_m^c + \varphi_m(t - \tau_0)) \tag{6}$$

$$E_m^{Y_l}(t) = \frac{A_m}{R_m^l}\cos(\omega_0 t - KR_m^l + \varphi_m(t - \tau_0)) \tag{7}$$

Based on the fact that antennas collecting the target radiation wave, the radio-frequency (RF) signals of each antenna element in array is derived as follows

$$E_{X_c}(t) = \sum f_{X_c}(x_m, y_m) E_m^{X_c}(t) \tag{8}$$

$$E_{Y_l}(t) = \sum f_{Y_l}(x_m, y_m) E_m^{Y_l}(t) \tag{9}$$

Where (x_m,y_m) is the corresponding coordinates of S_m. $f_{\#}(\bullet)$ is the normalized antenna pattern of antenna #. Then the RF signals from the antennas are amplified and shifted to intermediate frequency (IF) signals. For the ideal receivers with the same local oscillator, the I/Q signals output by these receivers can be represented as

$$EI_{X_c}(t) = E_{X_c}(t) \otimes \cos(\omega_{lo} t) = \sum f_{X_c}(x_m, y_m) \frac{A_m}{R_m^c}\cos(\omega_{if} t - KR_m^c + \varphi(t - \tau_0)) \tag{10}$$

$$EQ_{X_c}(t) = \sum f_{X_c}(x_m, y_m) \frac{A_m}{R_m^c}\cos(\omega_{if} t - KR_m^c + \varphi(t - \tau_0) - \frac{\pi}{2}) \tag{11}$$

$$EI_{Y_l}(t) = \sum f_{Y_l}(x_m, y_m) \frac{A_m}{R_m^l}\cos(\omega_{if} t - KR_m^l + \varphi(t - \tau_0)) \tag{12}$$

$$EQ_{Y_l}(t) = \sum f_{Y_l}(x_m, y_m) \frac{A_m}{R_m^l}\cos(\omega_{if} t - KR_m^l + \varphi(t - \tau_0) - \frac{\pi}{2}) \tag{13}$$

Where ω_{lo} is the local oscillator frequency, $\omega_{if} = \omega_0 - \omega_{lo}$ is the center frequency of intermediate frequency signals. Then the visibility function can be calculated by the cross-correlation between these IF signals.

$$VI(X_c, Y_l) = < EI_{X_c} \bullet EI_{Y_l} >_{T\tau} + < EQ_{X_c} \bullet EQ_{Y_l} >_{T\tau} \tag{14}$$

$$VQ(X_c, Y_l) = < EI_{X_c} \bullet EQ_{Y_l} >_{T\tau} - < EQ_{X_c} \bullet EI_{Y_l} >_{T\tau} \tag{15}$$

Where $< E(t) >_{T\tau} = \int_0^{T\tau} E(t) \Big/ T\tau$ denotes time integration operation. Now, the complex visibility function $V(c,l)$ can be calculated by the following formula

$$V(c,l) = VI(X_c, Y_l) - iVQ(X_c, Y_l) \tag{16}$$

Different from the far-field imaging, the near-field synthetic aperture imaging has a special phase-modified item, which is very important for the near-field SAIR. So we should improve the visibility function $V(c,l)$ and calculate the compensated visibility function $V_c(c,l)$.

$$V_c(c,l) = V(c,l)\exp[K(Y_l^2 - X_c^2)/2R] \tag{17}$$

The Eq. (17) is the final output results of this imaging model. Then the millimeter wave images with high resolution can be reconstructed by the relevant imaging algorithm from this compensated visibility function.

3. Signal-level Simulation and Analysis

To validate the modeling of the part-2, the signal-level simulation experiments are conducted by using the proposed model with the following parameters: System center frequency and wavelength are 94GHz and 3.2mm respectively, IF bandwidth is 100MHz, sampling rate of 250MHz, integration time ($T\tau$) is 1ms, antenna array is 100×100, antenna spacing is about 4λ, antenna element is round horn with diameter of 12mm, imaging distance is 5m.

3.1. The Target Radiation Signals

Here, the 1D simulation experiments with four point targets are performed to validate the signal-level effectiveness of the proposed model. The target locations are shown in Figure 4. The amplitudes A_m of these four targets are 1.0. In this imaging simulation model, target radiation waveforms are given as Eq. (1), where $\varphi_m(t)$ are set as statistical independent random sequence with the range of [-π, π]. It is the unique characteristics for the system to identify the target in the subsequent simulation process. Thus target radiation waveform $E_m(t)$ and probability distribution of the target S_m are shown in the Figure 2.

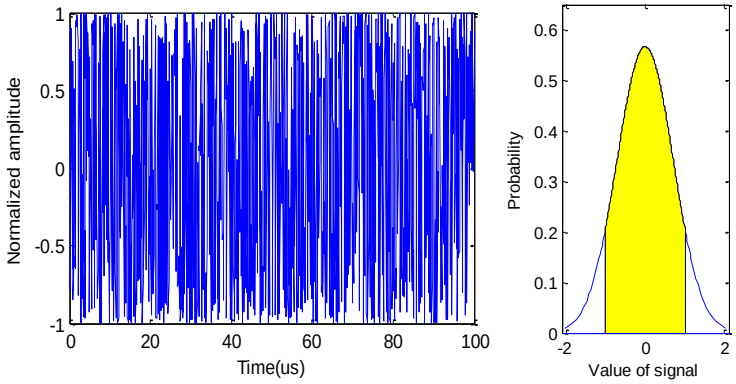

Figure 2. The Target Radiation Signal of Target 1: (a) Time Waveform of Target Radiation, (b) Probability Distribution

As Figure 2 shows, we can see that the target radiation signal is a random sequence with Gaussian distribution, whose mean and mean square are 0 and $A_m^2/2$ respectively [17, 18]. To compare the simulation results with theoretical results and analysis the

mutual coherence between point sources, the cross-correlation value of different targets are calculated by

$$I(m,n) = < E_m \bullet E_n >_{T\tau} \tag{18}$$

When $m=n$, $I(m,m)$ is the mean square of S_m. And the corresponding $I(m,n)$ is the cross-correlation value between the sources S_m and S_n. The results are shown in Table 1.

Table 1. Cross-correlation Values of Point Targets

Cross-correlation with 1ms/3ms		Targets			
		1	2	3	4
Targets	1	0.5014/0.5008	-0.0011/0.0007	0.0036/0.0015	0.0011/0.0003
	2	……	0.5155/0.5047	-0.0009/0.0005	-0.0021/0.0009
	3	……	……	0.4949/0.5011	0.0024/-0.0013
	4	……	……	……	0.4906/0.4979

Table1 shows that the autocorrelation value of the targets are close to their mean square $A_m^2/2$, and the cross-correlation values are close to zero as theoretical results. For comparison, the cross-correlation values are also calculated under the integration time of 3ms. Clearly, the results with 3ms integration time are more accurate than the results with 1ms integration time. These are consistent with the theoretical analysis.

3.2. The IF Signals of Antenna Elements

Considering that the IF signals are linear combination of all radiation signals of the point sources and the fact that responses of linear time-invariant system will be a stationary complex random process if the input is stationary complex random processes [18], the IF signals should have the same distribution with target radiation. According to Eq. (10-13), I/Q signals (*EI*s and *EQ*s) of the antenna elements are collected by the combination of all target radiation signals. The corresponding results (I/Q signals and their probability distribution) are shown in Fig. 3. The mean and mean square of IF signals are obtained by performing mean on both sides of Eq. (10-13).

$$\begin{aligned} \overline{EI_{X_c}(t)} &= \overline{\sum f_{X_c}(x_m, y_m) E_m^{X_c}(t)} \\ &= \sum f_{X_c}(x_m, y_m) \overline{E_m(t - KR_m^c / \omega_0)} = 0 \end{aligned} \tag{19}$$

$$\begin{aligned} \overline{|EI_{X_c}(t)|^2} &= \overline{\sum f_{X_c}^2(x_m, y_m) |E_m^{X_c}(t)|^2} \\ &\approx \sum f_{X_c}^2(x_m, y_m) A_m^2 / (2R_0^2) \end{aligned} \tag{20}$$

Where R_0 is the approximate distance, which is set as $c \times \tau_0$. When the size of the antenna element is small enough, the antenna pattern f#() can be ignored. And the mean square can be approximately represented as

$$\overline{|EI_{X_c}(t)|^2} \approx \sum A_m^2 / (2R_0^2) \tag{21}$$

We select five antennas (1~5) from the middle area of antenna array. Then the mean and mean square of the I/Q signals, and the cross-correlation values (*VI* and *VQ*) of them for each other are measured from the corresponding simulation results obtained by the Eq.(12-13). The corresponding results are shown in Table 2.

Table 2. The Numerical Results of the IF Signals of Antenna 1~5

Antenna element	1_I/Q	2_I/Q	3_I/Q	4_I/Q	5_I/Q
Mean	-0.0022/-0.0024	-0.0016/-0.0016	0.0010/-0.0021	-0.0021/-0.0008	0.0021/0.0015
Mean square	0.0825/0.0789	0.0796/0.0823	0.0796/0.0823	0.0813/0.0803	0.0796/0.0808
Cross-correlation	-0.0039	0.0018	0.0026	0.0012	0.0014
Error of variance (%)	3.125/1.375	0.500/2.875	0.500/2.875	1.625/0.375	0.500/1.000

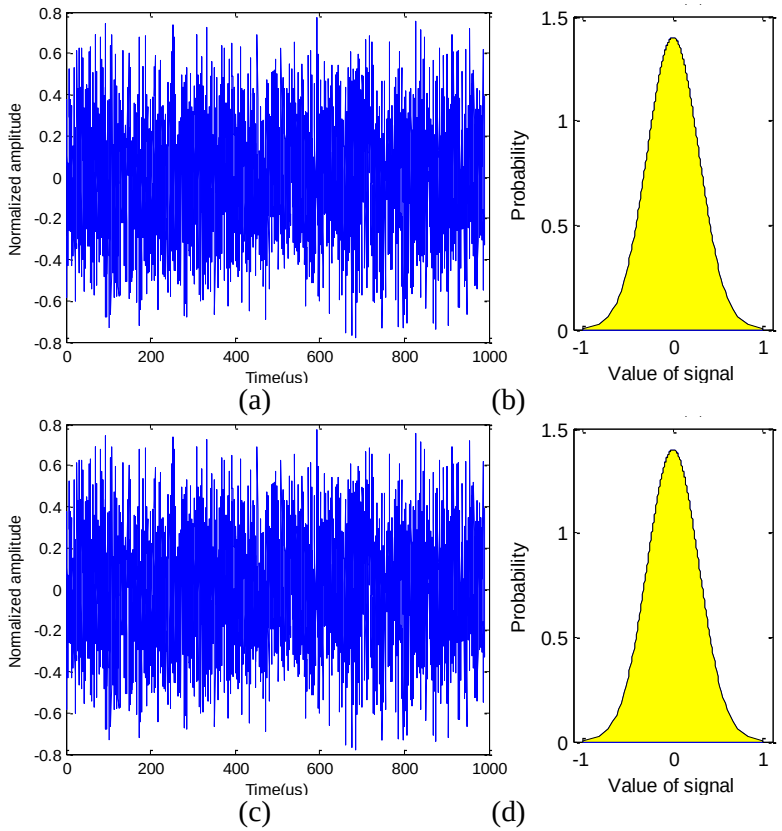

Figure 3. The IF Signals of Antenna c/I: (a) Time Waveform of I Signal, (b) Probability Distribution of I Signal, (c) Time Waveform of Q Signal, (d) Probability Distribution of Q Signal

Figure 3 and Table 2 show that I/Q IF signals of antenna elements are random sequences with 0-mean Gaussian distribution. The cross-correlation values between I and Q signals of the selected antenna 1~5 are all close to zero, this is in agreement with the fact that I/Q signals are orthogonal to each other. Consequently, the IF signals of all antennas have the same distribution. Table 2 also shows that the mean square of output signal sequences of antenna element 1~5 are all close to the theoretical result $2(A_m/R)^2$, which should be 0.08. The relative error of mean square is in the range [3.125%, 0.500%]. This slight difference is mainly due to the partial coherence between targets and the differences of antenna position. This error can be degraded by enlarging the size of antenna element and increasing the integration time. Hence, it can be concluded that output signal sequences of antenna array are in good agreement with theoretical result.

4. System-level Simulation and Analysis

For further validating the effectiveness of this model, the system-level imaging simulation experiments are conducted under the above parameters. There are numerous imaging methods designed to reconstruct the millimeter wave images for the compensated visibility function V_c [14, 19-20]. In this paper, we use the accurate imaging algorithm proposed in [14] to reconstruct the millimeter wave images. According to the above simulation parameters, the synthetic aperture (D_{SA}) is 1.28m×1.28m. Then the spatial resolution (ΔL) and no-aliasing FOV (L_{FOV}) can be calculated by the following formula

$$\Delta L = R \bullet \lambda / D_{SA} = \frac{5*0.0032}{1.28} = 1.25cm \tag{21}$$

$$L_{FOV} = R \bullet \lambda / \Delta d = \frac{5*0.0032}{4*0.0032} = 1.25m \tag{22}$$

4.1. The Imaging Simulation Experiments with 1D Targets

Firstly the four point targets analyzed above are reconstructed. For validating the spatial resolution of this model, target locations are set as (-0.0125,0), (0,0), (0.0250,0) and (0.0625,0) respectively. The distances between the targets are ΔL, $2\Delta L$ and $3\Delta L$ respectively. Target scene and corresponding imaging result are shown in Figure 4.

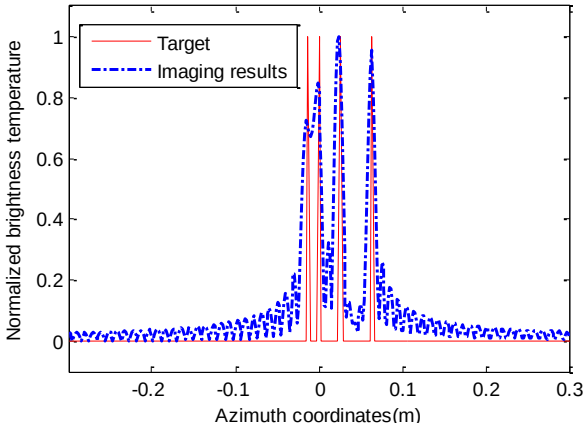

Figure 4. The Reconstructed Image of the Four Point Targets

The result shows that this simulation model can be used to simulate the point target imaging. The amplitudes and azimuths of the four point targets are reconstructed by the accurate imaging algorithm based on this imaging model accurately. As Figure 4 shows, even though the distance between targets is very close or equal to the spatial resolution (ΔL), this imaging model can also distinguish them with partial aliasing, which is inevitable for this imaging model similar to the real SAIR. Thus, by this imaging simulation experiment, we can draw the conclusion that the spatial resolution of this imaging model is equal to the theoretical spatial resolution of near-field millimeter wave SAIR approximately.

Then a simulation experiment with extended targets is demonstrated to verify the no-aliasing FOV of the proposed imaging model. As Figure 5 shows, the simulation target consists of three parts: the right section is an ideal triangle wave, the middle section is

the 1D truncation drawn from an actual gray image, and the left section is an ideal rectangular wave. The simulation results are shown in Figure 5.

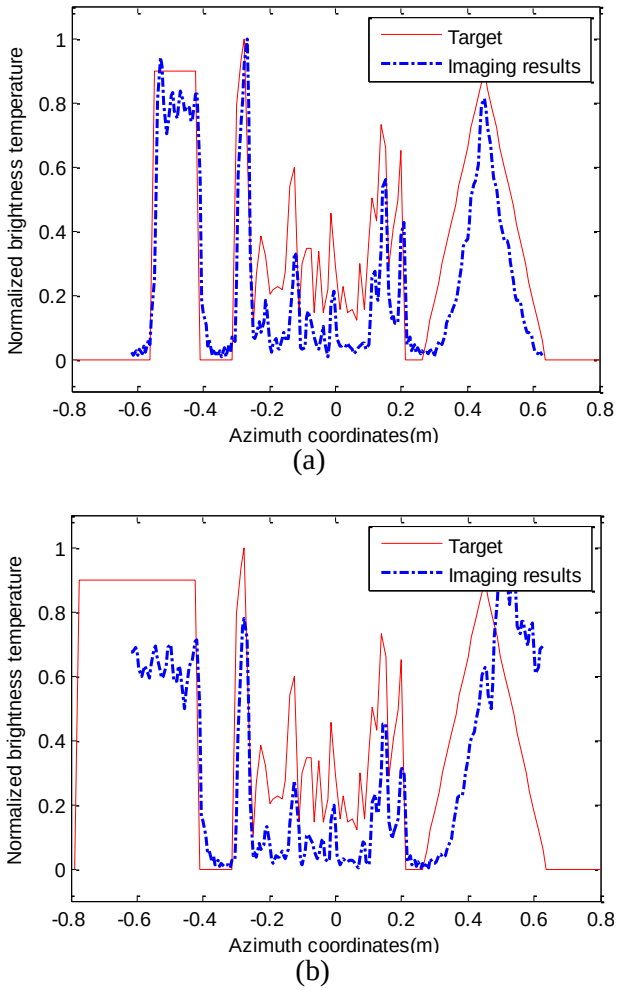

Figure 5. The Simulation Results of Extended Targets: (a) The Simulation Experiment without Aliasing, (b) The Simulation Experiment with Aliasing

As Figure 5 shows, when the target is smaller than the no-aliasing FOV [-0.625m 0.625m], the extended target can be reconstructed very well. But for the larger target with the extended triangle, there is a serious target aliasing phenomenon just as the frequency aliasing in the Nyquist sampling theory. By this simulation experiment, the no-aliasing FOV of SAIR and the effectiveness of this imaging model are verified well.

4.2. The Imaging Simulation Experiments with 2D Targets

For further validating the effectiveness of this model, a 2D imaging simulation experiment is performed here for demonstrating 2D imaging effectiveness of the proposed model. The target scene (brightness temperature) distribution is shown in Fig. 6, with its gray values as the radiation intensity (amplitudes) of the discrete radiation sources, and the distance between the point radiation sources is set as a half of system

spatial resolution (0.625 cm). The target dimension is set as 200×200. Thus, the target size is equal to the no-aliasing FOV of this imaging model (1.25m×1.25m).

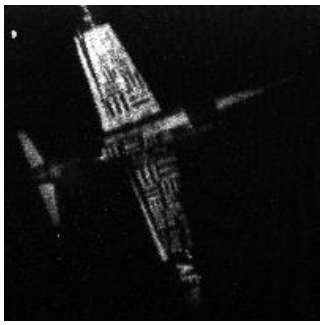

Figure 6. Brightness Temperature Distribution

Just as the 1D simulation experiment, the compensated visibility function is calculated based on the proposed simulation model firstly. Then the 2D target is reconstructed by the accurate imaging algorithm from the visibility function V_c. The corresponding result is shown in Figure 7.

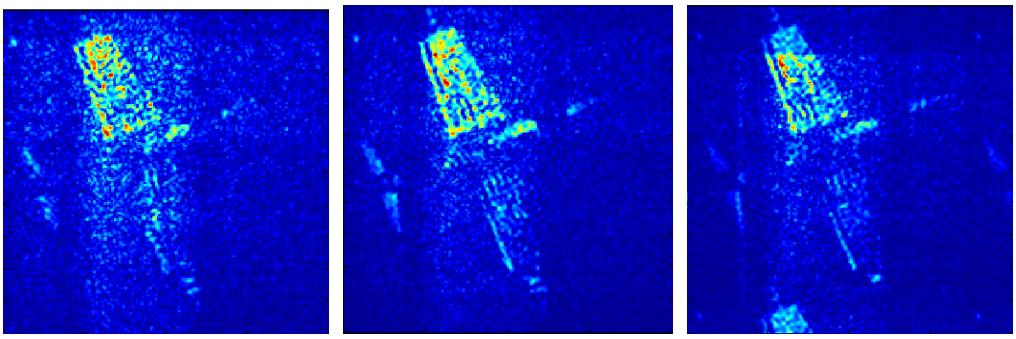

(a) (b) (c)

Figure 7. The Simulation Experiments with 2D Target Scene based on the Proposed Model: (a) Result with Integration Time 1ms, (b) Result with Integration Time 3ms, (c) Result with Target Aliasing

Figure 7(a) shows the imaging results of the target (airplane) based on the proposed model with integration time 1ms. Due to the fact that the partial coherence between targets is serious when the integration time is too small, there are a lot of noises near the target especially for the above-wing with high brightness temperature. We know that the partial coherence can be reduced by increasing the integration time obviously. So we demonstrate another 2D simulation with the same simulation parameters but the integration time ($T\tau$) is 3ms. The corresponding result is shown in Figure 7(b). It is obvious that the airplane is reconstructed more clearly than Figure 7(a). And the noise caused by the partial coherence is eliminated very well. In addition, we increase the target size to 1.5m×1.5m, which is larger than no-aliasing FOV. The imaging result is shown in Figure 7(c). Clearly, there is a serious aliasing phenomenon for this larger target just as expected. These simulation results demonstrate that the proposed model is an efficient, accurate imaging simulation model, and can be employed in the system design of near-field millimeter wave SAIR.

5. Conclusion

Under the background that theoretical analysis and instrument construction for antenna array of SAIR are both complicated, and designers usually hope to predict the imaging effect and analysis the parameters of SAIR before the system design. This paper presents an accurate imaging model of near-field millimeter wave SAIR for simulating the imaging process that include target radiating electromagnetic waves, antenna collecting target radiation and transforming them into IF signals, and antenna array collecting the visibility function. The signals are described in the time domain. They are very close to the realistic signals transformation of SAIR. This improves the efficiency of this simulation model significantly. For verifying the validity of the proposed model, the 1D and 2D simulation experiments are performed respectively. The simulation results show that this model can simulate the imaging process of near-field SAIR accurately. Besides, the proposed model cannot only be used in near-field millimeter wave SAIR, but also be suitable for other SAIR. We will further study the relevant parameters to improve the efficiency and expand the application of this simulation model.

Acknowledgements

The authors would like to thank the anonymous reviewer and editors for their helpful comments and suggestions. This work is supported by National (Jiangsu) Natural Science Foundation of China under Grants 61001010 and 60901008 (BK2010490), National Ministry Foundation of China under Grants 51305050102.

References

[1] R. Appleby and R. N. Anderton, "Millimeter-Wave and Submillimeter-Wave Imaging for Security and Surveillance," Proceedings of the IEEE, vol. 95, no. 8, **(2007)**, pp. 1683-1690.
[2] L. Yujiri, M. Shoucri, and P. Moffa, "Passive millimeter wave imaging," IEEE Microwave Magazine, vol. 4, no. 3, **(2003)**, pp. 39-50.
[3] D. M. Sheen, D. L. McMakin, and T. E. Hall, "Three-dimensional millimeter-wave imaging for concealed weapon detection," IEEE Trans. Microwave Theory and Techniques, vol. 49, no. 9, **(2001)**, pp. 1581-1592.
[4] C. Zheng, X. Yao, A. Hu and J. Miao, "A Passive Millimeter-Wave Imager Used for Concealed Weapon Detection," Progress In Electromagnetics Research B, vol. 46, **(2012)**, pp. 379-397.
[5] C. S. Ruf, C. T. Swift, A. B. Tanner, and D. M. Le Vine, "Interferometric synthetic aperture microwave radiometry for the remote sensing of the Earth," IEEE Trans. Geoscience and Remote Sensing, vol. 26, no. 5, **(1998)**, pp. 597-611.
[6] D. M. Le Vine and J. C. Good, "Aperture synthesis for microwave radiometers in space," NASA Tech. Memo. 85033, Goddard Space Flight Center, Greenbelt, MD, **(1983)**.
[7] M. D. Le Vine, M. Kao, B. A. Tanner, T. C. Swift and A. Griffis, "Initial results in the development of a synthetic aperture microwave radiometer," IEEE Trans. Geoscience and Remote Sensing, vol. 28, **(1990)**, pp. 614-619.
[8] M. D. Le Vine, and M. Haken, "RFI at L-band in synthetic aperture radiometers," Proceedings of IGARSS, vol. 3, (**2003**), pp. 1742-1744.
[9] M. Martín-Neira, S. Ribó, and J. A. Martín-Polegre, "Polarimetric mode of MIRAS," IEEE Trans. Geoscience and Remote Sensing, vol. 40, no. 8, **(2002)**, pp. 1755-1768.
[10] [A. Camps, J. Bara, I. C. Sanahuja, and F. Torres, "The processing of hexagonally sampled signals with standard rectangular techniques: Application to 2-D large aperture synthesis interferometric radiometers," IEEE Trans. Geoscience and Remote Sensing, vol. 35, no. 1, **(1997)**, pp. 183-190.
[11] A. Camps, Application of interferometric radiometry to earth observation. in Department of Signal Theory and Communication, vol. Ph.D. Barcelona, Spain: Univ. Politecnica de Catalunya, **(1996)**.
[12] I. Corbella, A. Camps, M. Zapata, F. Marcos, F. Martínez, F. Torres and J. Bará, "End-to-end simulator of two-dimensional interferometric radiometry," Radio Sci. vol. 38, no. 3, **(2003)**, pp. 23-1-8.

[13] Y. Li, J. Dong, K. Chen and W. Guo, "Signal level simulation modeling for antenna array of aperture synthesis radiometer based on the equivalent complex basedband representations," Journal of Infrared, Millimeter, and Terahertz Waves, vol. 29, no. 7, **(2008)**, pp. 663-672.
[14] J. Chen, Y. Li, J. Wang, Y. Li and Y. Zhang, "An accurate imaging algorithm for millimeter wave synthetic aperture imaging radiometer in near-field," Progress In Electromag. Research, vol. 141, **(2013)**, pp. 517-535.
[15] T. F.Ulaby, R. K. Moore, and A. K. Fung, "Microwave Remote Sensing: Microwave remote sensing fundamentals and radiometry", Addison-Wesley publishing company, advanced book Program/world science division **(1981)**.
[16] M. Born and E. Wolf, "Principles of optical", London. Cambridger univercity press, **(1999)**.
[17] B. Davis, E. Kim, and J. R. Piepmeier, "Stochastic modeling and generation of partially polarized or partially coherent electromagnetic waves," Radio Sci., vol. 39, no.1, **(2004)**, RS1001 Jan.
[18] Z. Shu Jie, and Z. Jian Jun, "Theory of Signal Detection and Estimation", Tsinghua University Press, Beijing, **(2005)**.
[19] N. Duffo, I. Corbella, F. Torres A.Camps and M. Vall-llossera, "Advantages and drawbacks of near field characterization of large aperture synthesis radiometers," 8th Specialist Meeting on Microwave radiometry and Remote Sensing Applications. University La Sapienza, Rome, **(2004).**
[20] B. A. Tanner, H. B. Lambrigsten, M. T. Gaier and F. Torres, "Near field characterization of the GeoSTAR demonstrator," Proc. of IEEE Int'l Geoscience and Remote Sensing Symposium, Denver, Co, USA, **(2006)**.

Authors

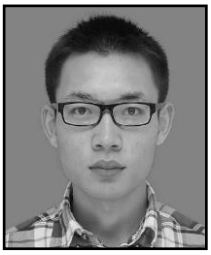

Jianfei Chen, he was born in Jiang Su, China, in1987. He received the B.Eng. degree in Electronic information science and technology from the Haerbin University of Science and Technology, Haerbin, China, in 2009, and is currently working toward the Ph.D. degree at Nanjing University of Science and Technology (NUST) Nanjing, China.

His research interests include signal processing and millimeter-wave imaging technology, the analysis and design of millimeter-wave synthetic aperture imaging radiometer.

Yuehua Li, he received the Ph.D. degree in electrical engineering technology from Nanjing University, Nangjing, China, in 1997.

He is currently a Professor with the School of Electronic Engineering and Optoelectronic Technology, and an Associate director with the research institute of millimeter wave and light wave proximity sensing, Nanjing University of Science and Technology. He has authored or coauthored over 80 journal and conference papers. He has submitted four patent applications. His current research interests include microwave and millimeter-wave theories and technologies, microwave and millimeter-wave detection, multimode compound detection and signal detecting and processing. Prof. Li was a six-time recipient of the Ministerial and Provincial-Level Science and Technology Award.

Jianqiao Wang is PhD student, School of Electronic Engineering and Optoelectronic Technology, Nanjing University of Science and Technology, Nanjing, China.

Yuanjiang Li, he is a doctor of Information and Communication Engineering, School of Electronic Engineering and Optoelectronic Technology, Nanjing University of Science and Technology, Nanjing, China.

